

Evaluation of Single-Frequency Precise Point Positioning Performance Based on SPARTN Corrections Provided by the SAPCORDA SAPA Service

Yeong-Guk Kim^{1,2}, Hye-In Kim², Hae-Chang Lee¹, Miso Kim², Kwan-Dong Park^{1,2}

¹Department of Geoinformatic Engineering, Inha University, Incheon 22212, Korea

²PP-Solution Inc., Seoul 08504, Korea

ABSTRACT

Fields of high-precision positioning applications are growing fast across the mass market worldwide. Accordingly, the industry is focusing on developing methods of applying State-Space Representation (SSR) corrections on low-cost GNSS receivers. Among SSR correction types, this paper analyzes Safe Position Augmentation for Real Time Navigation (SPARTN) messages being offered by the SAfe and Precise CORrection DAta (SAPCORDA) company and validates positioning algorithms based on them. The first part of this paper introduces the SPARTN format in detail. Then, procedures on how to apply Basic-Precision Atmosphere Correction (BPAC) and High-Precision Atmosphere Correction (HPAC) messages are described. BPAC and HPAC messages are used for correcting satellite clock errors, satellite orbit errors, satellite signal biases and also ionospheric and tropospheric delays. Accuracies of positioning algorithms utilizing SPARTN messages were validated with two types of positioning strategies: Code-PPP using GPS pseudorange measurements and PPP-RTK including carrier phase measurements. In these performance checkups, only single-frequency measurements have been used and integer ambiguities were estimated as float numbers instead of fixed integers. The result shows that, with BPAC and HPAC corrections, the horizontal accuracy is 46% and 63% higher, respectively, compared to that obtained without application of SPARTN corrections. Also, the average horizontal and vertical RMSE values with HPAC are 17 cm and 27 cm, respectively.

Keywords: SSR, SPARTN, SAPCORDA, PPP-RTK, code-PPP

1. INTRODUCTION

Responding to the increasing need for high-precision localization across numerous markets, high-precision positioning technologies based on Global Navigation Satellite System (GNSS) are being developed and implemented. Unmanned vehicles including self-driving automobiles and

drones, known as the key technology of the Fourth Industrial Revolution, is one of the growing markets. The general public is also using more Location Based Service (LBS) applications in diverse parts of daily life. Thus, the industry is focusing on high-precision GNSS researches according to the rising demand from the mass market.

There are two conditions for the mass market to fully utilize high-precision positioning. First, the correction data service, which is vital to improving positioning accuracy, should be available to a large number of users without significant barriers. Second, the receiver price should be reasonable so that the user can easily afford it. Accordingly, the GNSS industry is seeing a growth in developing State Space Representation (SSR) corrections applied on low-cost receivers.

In SSR-based positioning, the service provider collects real-time GNSS observations from the reference network

Received Feb 05, 2021 Revised Feb 24, 2021 Accepted Mar 03, 2021

†Corresponding Author

E-mail: hikim@ppsoln.com

Tel: +82-2-6925-1516 Fax: +82-2-6455-4305

Yeong-Guk Kim <https://orcid.org/0000-0003-4770-813X>

Hye-In Kim <https://orcid.org/0000-0002-3256-9037>

Hae-Chang Lee <https://orcid.org/0000-0002-3133-2871>

Miso Kim <https://orcid.org/0000-0002-6959-1991>

Kwan-Dong Park <https://orcid.org/0000-0003-1538-8768>

and models each error component individually and then transmits the corresponding error information to the user. Usually, SSR messages contain corrections for five error terms: satellite orbit error, satellite clock error, satellite signal bias, ionospheric delay, and tropospheric delay. The data transfer is more efficient than the traditional Observation Space Representation or OSR method because error corrections are separated according to each error source (Kim 2016). In addition, the number of users is unlimited because two-way communication is not necessary. Due to such features, SSR correction is recognized as a viable solution for precise positioning service aimed at handling unlimited number of users. Positioning techniques utilizing SSR corrections are SBAS, PPP, and PPP-RTK, which are distinguished according to the kind of GNSS observation and correction types used.

Although GNSS positioning based on SSR messages is acknowledged as one of the key technologies that meet the market demand for high-accuracy localization, its international standard is being made and has not been finalized. Therefore, most of the current SSR service providers choose their own proprietary format and do not open the specifics to the public. Services like CenterPoint RTX by Trimble, Seastar by Fugro, and StarFire by Navcom are some examples of un-disclosed formats. SSR transmission standards that are open, on the other hand, are Compact SSR by Japan's QZSS (Japan Cabinet Office 2020), SSRZ by Germany's Geo++ (Geo++ 2020), and Safe Position Augmentation for Real Time Navigation (SPARTN) by Safe and Precise CORrection DATA (SAPCORDA).

The leading company in the affordable GNSS module and chipset market, u-blox, has created a joint venture called SAPCORDA with Bosch, Geo++, and Mitsubishi Electric in August 2017. This venture focuses on developing SSR correction service, which they named Safe And Precise Augmentation Service (SAPA). The SSR format provided through SAPA is called SPARTN (SAPCORDA 2020a). Vana et al. (2019) conducted a research on GNSS correction services for high-precision GNSS positioning suitable for automotive applications. The research focused on analyzing SPARTN messages and compared SSR and Compact SSR protocols. They found that horizontal positioning accuracy with SPARTN messages was 0.8–1.6 m for the initial 20 seconds. After reaching convergence in about 30 seconds, the horizontal accuracy improved to better than 10 cm, with Root Mean Square Error (RMSE) of 4.5 cm. However, the research paper does not provide details on data processing methods nor positioning accuracy analysis. Other than this article, we could not find any other journal publication on GNSS processing utilizing SPARTN SSR messages.



Fig. 1. SAPA service coverage (SAPCORDA SAPA Service 2021).

This paper introduces the SPARTN message field structure and summarizes the essential procedures of converting SPARTN messages to the range measurement error. Especially, differences between Basic-Precision Atmosphere Correction (BPAC) and High-Precision Atmosphere Correction (HPAC) are described in detail. In the second half, Code-PPP and ambiguity-float PPP-RTK positioning results obtained with single-frequency GPS measurements are analyzed.

2. OVERVIEW OF SPARTN

SAPCORDA SAPA service provides SSR corrections in SPARTN format. According to SAPA datasheet Version 1.4, SSR corrections are broadcasted through the Internet or Geostationary Satellite L-Band with a continental data rate of 2400 bps (SAPCORDA 2020b). As shown in Fig. 1, as of today, the SAPA service covers all the major European regions and the continental U.S.A and plans to broaden the target area globally. There are three types of SAPA services depending on the positioning accuracy it provides: Basic, Premium, Premium+. SAPA Basic is a service for PPP and the horizontal accuracy is 30 cm to 1 m at 2-sigma (95%). SAPA Premium and Premium+ are for PPP-RTK with an improved horizontal accuracy that is better than 10 cm at 2-sigma. Overall, Premium and Premium+ are high-precision services that allow convergence within 10 seconds while providing horizontal accuracy of 3 cm to 6 cm. This is reachable under the conditions of using error-free GNSS observation data, receiving complete and uninterrupted SAPA correction data, and utilizing ambiguity-fixed positioning. The difference between Premium and Premium+ is that integrity messages are added in the "Premium+" service. Details of each service type is listed in Table 1.

The SPARTN standard format gets updated based on collaborations among participating companies and interoperability tests. Bosch, Geo++, Mitsubishi Electric, Septentrio, and u-blox are the partners that cooperate in this research collaboration. Details of the format are published in SPARTN Interface Control Documentation (ICD) documents. Version 1.8 of the ICD is freely available on the web and

Table 1. Key features of SAPA service (SAPCORDA SAPA Service 2021).

Grade	SAPA basic	SAPA premium	SAPA premium+
Accuracy	10 cm ~ 1 m	~ 10 cm	~ 10 cm
Coverage	Europe, USA	Europe, USA	Europe, USA
Data format	SPARTN	SPARTN	SPARTN
Type of stream	Broadcast	Broadcast	Broadcast
Integrity	N/A	N/A	Included
e.g	Mobile / IoT	Logistics or mobile / IoT	Automotive / New mobility, Autonomous airborne systems

Table 2. SPARTN correction message types and descriptions (SAPCORDA 2020a).

Type	Subtype	Message name	Description
0	0	GPS OCB	GNSS orbit, clock, bias
	1	GLONASS OCB	
	2 to 15	TBD	
1	0	GPS HPAC	High-precision atmosphere correction
	1	GLONASS HPAC	
	2 to 15	TBD	
2	0	GAD	Geographic area definition
	1 to 15	TBD	
3	0	BPAC polynomial	Basic-precision atmosphere correction
	1 to 15	TBD	
4	0	Dynamic key message	Encryption and authentication support
	1	Group authentication message	
	2 to 15	TBD	
5 to 127	TBD	TBD	TBD



Fig. 2. Message frame layout (SAPCORDA 2020a).

version 2.0 is being provided upon request. The former version includes only GPS and GLONASS corrections, while the latter added additional signals, GNSS constellations, and integrity messages (SPARTN Format 2021). Users can easily decode SPARTN messages following the definitions described in the ICD document.

3. SPARTN CORRECTION

3.1 SPARTN Messages

Each SPARTN message frame has five sections as shown in Fig. 2, and the whole frame consists of 18 Transport-layer Field (TF): TF001 through TF018. The third section “Payload” contains error corrections needed for positioning.

Correction messages in TF016, the Payload, consists of Types 0 through 127. Types 0 through 4 are currently in use. Type 4 is about message encryption and authentication, so the necessary information for positioning error corrections is included in Types 0, 1, 2, and 3. The correction message types and descriptions are listed in Table 2. SPARTN correction is divided into four types: Type 0 is about satellite orbit, clock, and bias errors; Type 1 is HPAC; Type 2 is Geographic Area Definition; and Type 3 is BPAC.

3.2 GNSS Orbit, Clock, Bias

The orbit correction term δO contains radial, along-track, and cross-track components in units of meters. By transforming δO to the Earth-Centered Earth-Fixed (ECEF) frame using Eq. (1), one can obtain δX . Then, as shown in Eq. (2), by subtracting δX from the broadcast satellite position X_b , one can calculate the corrected satellite position X_{orb} . In Eq. (1), e_i ($i = \text{radial, along, cross}$) is the direction unit vector.

$$\delta X = [e_{\text{radial}} \ e_{\text{along}} \ e_{\text{cross}}] \cdot \delta O \tag{1}$$

$$X_{\text{orb}} = X_b - \delta X \tag{2}$$

The clock correction δC is also provided in the unit of meter. Following the formula shown in Eq. (3), the corrected satellite clock t_s can be calculated by combining δC with broadcast satellite clock t_b . The term c in Eq. (3) is the speed of light constant.

$$t_s = t_b - \frac{\delta C}{c} \tag{3}$$

The magnitude of satellite bias correction is available in the unit of meter. Bias correction can be simply done by subtracting the corresponding bias term from the pseudorange and carrier phase measurements. The

Table 3. Comparison of HPAC and BPAC messages.

Components	HPAC (Type 1)	BPAC (Type 3)
Ionosphere data	STEC (polynomial co-efficient, grid residuals)	VTEC (Average VTEC, grid residuals)
Troposphere data	Zenith delay (Average zenith hydrostatic delay, polynomial co-efficient, grid residuals)	N/A
Area data	Type 2	Type 3

pseudorange and carrier phase measurement types defined in SPARTN version 1.8 are C1C, C2W, C2L, L1C, L2W, L2L for GPS, and C1C, C2C, L1C, L2C for GLONASS.

3.3 HPAC and BPAC

SPARTN provides ionospheric and tropospheric delay corrections through messages Type 1 HPAC and Type 3 BPAC, respectively. Differences between BPAC and HPAC are listed in Table 3. BPAC provides the ionospheric delay correction in units of Vertical Total Electron Content (VTEC) and does not include tropospheric delay corrections. On the other hand, HPAC contains tropospheric delay corrections and one should note that the ionospheric delay correction is provided as Slant TEC (STEC) instead of VTEC.

The slant ionospheric delay in the unit of meter is computed by using HPAC polynomial coefficients and grid residuals as in Eqs. (4) and (5). δI_{CP}^i in Eq. (4) is the slant ionospheric delay of satellite i , for the carrier phase measurement. δI_{PR}^i in Eq. (5) is slant ionospheric delay of satellite i , for the pseudorange measurement. I_p^i in Eqs. (4) and (5) is slant ionospheric delay evaluated for the polynomial for satellite i , whereas I_G^i is the interpolated residual slant ionosphere delay obtained from the gridded residuals. The unit for I_p^i and I_G^i in Eqs. (4) and (5) is TECU. A bi-linear grid interpolation is used to get I_G^i , which is the residual slant delay for the requested user position. The slant ionospheric delay I_p^i is computed using the distance between the user location and the area centroid in addition to the polynomial coefficient provided. More details can be found in SPARTN ICD.

$$\delta I_{CP}^i = -40.3 \times \frac{10^{-16}}{f_j^2} \cdot (I_p^i + I_G^i) \quad (4)$$

$$\delta I_{PR}^i = 40.3 \times \frac{10^{-16}}{f_j^2} \cdot (I_p^i + I_G^i) \quad (5)$$

BPAC provides area-specific average VTEC values and grid residuals at the ionosphere shell height. In Eq. (6), $VTEC_i$ is the VTEC of satellite i , $VTEC_{Avg}$ is the average VTEC within the area, and $VTEC_{Grid}$ is the VTEC residual of the specified location. Units of all VTEC values are TECU. As in Eq. (6), VTEC at each grid point is calculated by adding grid residuals to the average VTEC value. The user can compute

VTEC at the ionosphere pierce point (IPP) by interpolating VTEC values from the grids close to IPP and then convert the obtained VTEC value at IPP to STEC through a mapping function. More details on interpolation and transformation are available in SPARTN ICD.

$$VTEC_i = VTEC_{Avg} + VTEC_{Grid} \quad (6)$$

Tropospheric delay corrections are available only through HPAC, not BPAC. The tropospheric delay is computed as shown in Eq. (7). \overline{T}_h^Z is the average zenith hydrostatic delay for the given area referenced to the zero ellipsoidal height, T_p is the residual troposphere zenith delay for station interpolated obtained from the polynomial expansion, in units of meters. T_G is the residual troposphere zenith delay for station interpolated from the grid points, in units of meters. The notation $m_h(\epsilon_i, h)$ is the hydrostatic mapping function for the satellite elevation angle ϵ_i at the ellipsoidal height h of the approximate user location and $m_{nh}(\epsilon_i)$ is the non-hydrostatic mapping function for the satellite elevation angle (Niel 1996). T_p can be computed using polynomial coefficients and the distance between the user location and the area centroid. A bi-linear grid interpolation is used to calculate the residual T_G for the requested user position. More details can be found in SPARTN ICD.

$$\delta T^i = \overline{T}_h^Z m_h(\epsilon_i, h) + (T_p + T_G) \cdot m_{nh}(\epsilon_i) \quad (7)$$

Clarification on which area and grid point the correction is about is essential in applying the ionospheric and tropospheric delay correction to the user location. Such area definition is provided through Type 2 for HPAC and Type 3 for BPAC. Fig. 3 illustrates the grid layout of the area data, and BPAC and HPAC share the same structure. The area data includes "Area ID" which shows the area the correction refers to. The Area Reference Point (ARP) is defined to establish the grid layout. The grid node count and spacing for both longitude and latitude are provided with regards to the ARP coordinate. Among the green grid nodes, the first or upper left dot corresponds to ARP. The red dot is the polynomial expansion point which is used for calculation of the ionospheric and tropospheric delay based on HPAC polynomial coefficients.

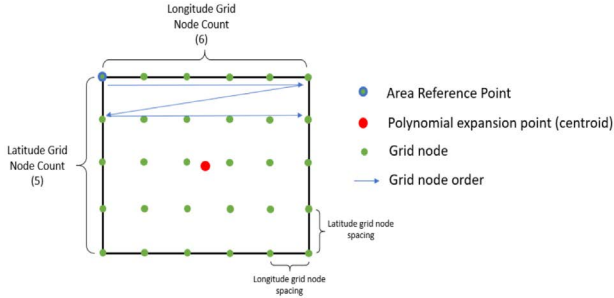


Fig. 3. SPARTN grid layout (SAPCORDA 2020a).



Fig. 4. Location of the SAPCORDA SCDE reference station.

4. POSITIONING ACCURACY ASSESSMENT WITH SPARTN

In this section, the positioning accuracy of SPARTN SSR correction was validated. We developed GPS Code-PPP and PPP-RTK post-processing algorithms based on single-frequency using the MATLAB software. While Code-PPP uses pseudorange measurements only, PPP-RTK processes pseudoranges and carrier phases together. Also, the PPP-RTK algorithm developed uses float ambiguity solutions, not fixed ones. The SPARTN SSR message utilized was broadcasted in Europe on Day of Year (DOY) 148 of year 2020 and this data was provided by SAPCORDA. The GPS data is 1-second interval measurements collected by the SCDE reference station on the same day. The SCDE reference station is located in Germany as seen in Fig. 4.

4.1 Code-PPP

In Code-PPP positioning, SSR corrections were combined with GPS single-frequency pseudorange observations. The site coordinate was computed at every second with least-squares estimation (LSE). The first 20-minute measurements at every hour were taken on DOY 148 of year 2020. Thus 24 datasets were tested to analyze the positioning accuracy. We compared results of three positioning scenarios: 1) without SSR corrections, 2) with BPAC corrections, and 3) with HPAC corrections. In this paper we denote each scenario as ‘SPP’, ‘BPAC’, and ‘HPAC’ for brevity. SPP stands for Standard Point Positioning, and BPAC and HPAC correspond to SPARTN correction types described in Section 3.

Eq. (8) is the Code-PPP pseudorange measurement equation between receiver r and satellite i . In the equation, p_r^i is the pseudorange measurement, ρ_r^i is the 3D distance between the receiver and the satellite, c is the speed of light, δt_r is the receiver clock offset, δt^i is the satellite clock offset, I_r^i is ionospheric delay, T_r^i is tropospheric delay, B_p^i is satellite code bias error, M_r^i is multipath error, and ε_p is pseudorange

Table 4. Error correction data and models for each Code-PPP positioning scenario.

	SPP	BPAC	HPAC
Orbit/Clock/Bias	N/A	Orbit/Clock/Bias	Orbit/Clock/Bias
Troposphere	GPT	GPT	HPAC
Ionosphere	Klobuchar	BPAC	HPAC

measurement noise.

$$p_r^i = \rho_r^i + c(\delta t_r - \delta t^i) + I_r^i + T_r^i + B_p^i + M_r^i + \varepsilon_p \quad (8)$$

Eq. (9) is the state vector for the Code-PPP estimation algorithm, and (x_r, y_r, z_r) are the coordinates of the receiver.

$$x = [x_r, y_r, z_r, \delta t_r] \quad (9)$$

In the case of SPP, orbit-clock-bias errors were not corrected for. Meanwhile, the tropospheric and ionosphere delay was accounted by Global Pressure and Temperature (GPT) by Boehm et al. (2007) and Klobuchar (1987) models, respectively. In the case of BPAC and HPAC, satellite orbit-clock-bias errors are corrected. Also, the ionospheric correction from BPAC and HPAC corrects the ionospheric delay. BPAC uses GPT to correct tropospheric delay and HPAC uses the tropospheric correction within HPAC. Error corrections and the corresponding models used for Code-PPP are listed in Table 4.

As the reference or true coordinate, we utilized the precise coordinates obtained from the web-based Automated Precision Positioning Service (APPS). The daily, 24-hour RINEX file obtained at the SCDE station on DOY 148 was uploaded to the APPS site to get the reference coordinate. The elevation cut-off angle was set to 12.5° in all three positioning modes. In the BPAC and HPAC processing, only those satellites whose SPARTN corrections are available were used. However, in the SPP model, all visible satellites were included in the data processing.

Fig. 5 shows Code-PPP horizontal errors processed from 12:00 to 12:20 among the 24 data sets: SPP is in red, BPAC in green, and HPAC in blue. SPP accuracy is the poorest and

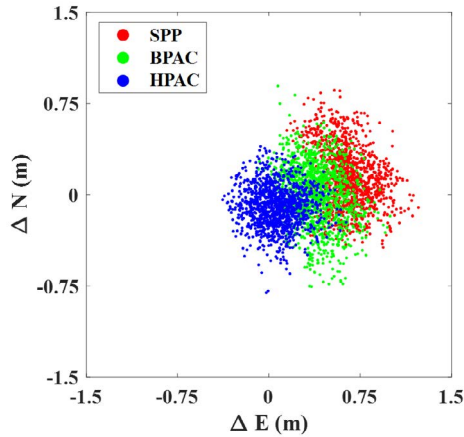


Fig. 5. Code-PPP horizontal accuracy comparison of each scenario on 12:00~12:20.

Table 5. Minimum, maximum, and average RMSE (m) from three Code-PPP positioning scenarios.

Scenario	Direction	Minimum	Maximum	Average
SPP	Horizontal	0.35	7.07	1.25
	Vertical	0.50	8.53	2.30
	3-dimension	0.70	8.81	2.76
BPAC	Horizontal	0.32	4.52	0.86
	Vertical	0.37	6.49	1.14
	3-dimension	0.64	7.92	1.45
HPAC	Horizontal	0.25	0.62	0.34
	Vertical	0.30	0.79	0.50
	3-dimension	0.42	0.84	0.61

HPAC accuracy is better than that of BPAC. The minimum, maximum, and average of every 24 RMSE of each scenario is listed in Table 5. The average horizontal RMS error is 1.25 m for SPP, 0.86 m for BPAC, and 0.34 m for HPAC. The average vertical RMS error also improves to 2.30 m, 1.14 m, and 0.50 m.

4.2 PPP-RTK

PPP-RTK positioning algorithm used HPAC corrections along with GPS single-frequency pseudorange and carrier phase observations. The site coordinate was estimated at every second with the Kalman Filter method. The datasets are the same as those used for Code-PPP in Section 4.1; the first 20-minute measurements at every hour were taken on DOY 148 of year 2020. Thus 24 datasets were tested to analyze the positioning accuracy. The same precise coordinates obtained from APPS were used to derive position errors. The elevation cut-off angle was set to 12.5°.

Eq. (10) is the carrier phase measurement equation: ϕ_r^i is the carrier phase measurement, B_ϕ^i is the satellite carrier bias error, ε_ϕ is the carrier phase measurement noise, λ is the wavelength, and N_r^i is an integer ambiguity. In this case of PPP-RTK, satellite orbit-clock-bias errors are corrected. Also,

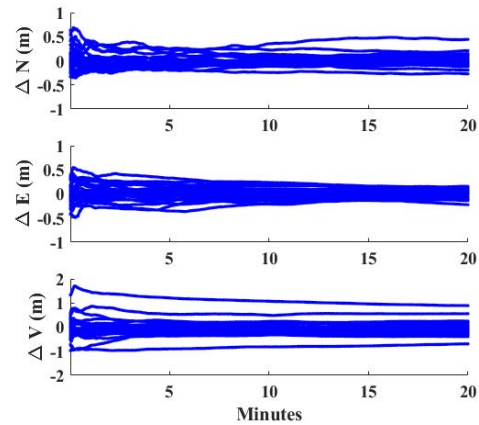


Fig. 6. PPP-RTK errors in the north, east, and vertical directions.

Table 6. PPP-RTK minimum, maximum, and average RMSE (m).

	Minimum	Maximum	Average
Horizontal	0.08	0.39	0.17
Vertical	0.04	1.12	0.27
3-dimension	0.15	1.13	0.34

the ionospheric and tropospheric delays are also corrected using HPAC.

$$\phi_r^i = \rho_r^i + c(\delta t_r - \delta t^i) - I_r^i + T_r^i + B_\phi^i + \lambda N_r^i + M_r^i + \varepsilon_\phi \quad (10)$$

Eq. (11) is the state vector of PPP-RTK algorithm. This paper estimates the integer ambiguity with a float solution.

$$x = [x_r, y_r, z_r, \delta t_r, N_r^1, N_r^2, \dots, N_r^{i-1}, N_r^i] \quad (11)$$

Fig. 6 shows PPP-RTK positioning result using HPAC corrections. In the figure, the coordinate deviations for every dataset are plotted as time-series in the north-south (North), east-west (East) and up (Vertical) directions. Table 6 categorized the statistics of all the 24 datasets. The average horizontal and vertical values are 17 cm and 27 cm, respectively. The dataset with the minimum error showed a horizontal error of 8 cm and vertical error of 4 cm. Fig. 7 depicts RMSE histogram by 5 cm bins. In the case of the horizontal direction, 22 of the 24 datasets have errors less than 30 cm and 17 datasets show errors less than 20 cm. As for the vertical error, 19 of the 24 datasets achieved accuracies better than 30 cm.

The average horizontal accuracy 17 cm, computed in Section 4.2, is poorer compared to that stated in Vana et al. (2019) and the SAPA datasheet. This is assumed to have happened due to the difference between the ambiguity-float solution and the ambiguity-fix solution. We believe that an accuracy better than the ambiguity-float will be achievable

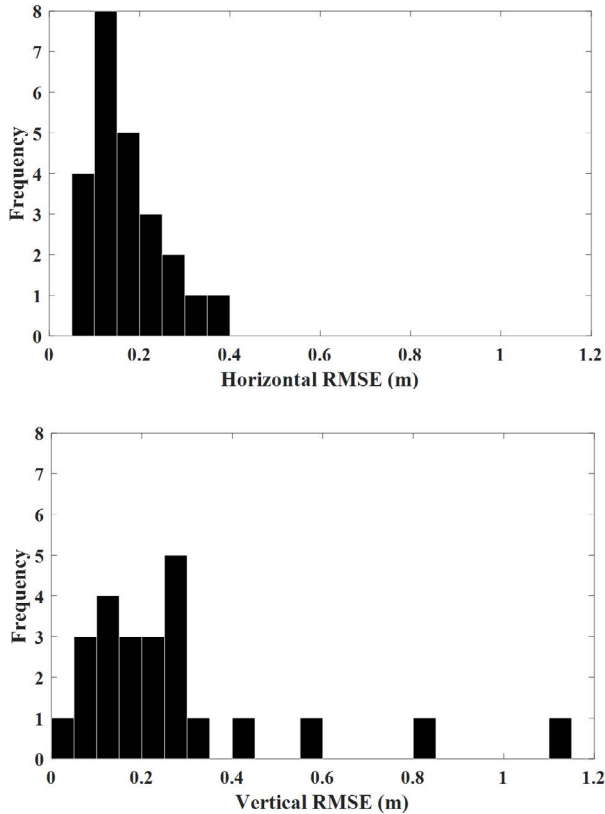


Fig. 7. PPP-RTK horizontal and vertical RMSE histogram.

when applying SPARTN message to the ambiguity-fixing algorithm.

Therefore, it can be concluded that precise positioning with an average of 17 cm horizontal accuracy is possible when SPARTN messages are applied to an ambiguity-float PPP-RTK algorithm, even with a single-frequency receiver.

5. CONCLUSIONS

First, the details and application procedures of SPARTN messages were introduced. We also developed and assessed Code-PPP and PPP-RTK algorithms that use SPARTN corrections. We compared three positioning scenarios of Code-PPP: SPP, processing with BPAC and processing with HPAC. With HPAC messages, the horizontal accuracy improved by 73% with respect to that of SPP. It also improved by 31% compared to that of BPAC messages. At the same time, the vertical accuracy got better by 78% and 50%, respectively. In the second part of algorithm validation, we used in-house ambiguity-float PPP-RTK positioning algorithms. From single-frequency Kalman filtered 1-second position estimates from 24 datasets, we found that average RMSEs in the horizontal and vertical directions are 17 cm

and 27 cm, respectively. Nevertheless, stable sub-decimeter positioning accuracies mentioned in the SAPA datasheet should be obtained when integer ambiguities are fixed.

ACKNOWLEDGMENTS

This work is supported by the Korea Agency for Infrastructure Technology Advancement (KAIA) grant funded by the Ministry of Land, Infrastructure and Transport (Grant 21CTAP-C163836-01). The authors appreciate Sapcorda for providing sample SPARTN messages and base station data.

AUTHOR CONTRIBUTIONS

Conceptualization, K.D. and Y.G.; methodology, Y.G. and H.I.; validation, Y.G.; formal analysis, Y.G. and M.S.; investigation, Y.G. and H.I.; resources, Y.G. and H.C.; data curation, Y.G. and H.C.; writing—original draft preparation, H.I.; writing—review and editing, K.D. and Y.G.; visualization, Y.G.; supervision, K.D.

CONFLICTS OF INTEREST

The authors declare no conflict of interest.

REFERENCES

- Boehm, J., Heinkelmann, R., & Schuh, H. 2007, Short Note: A global model of pressure and temperature for geodetic applications, *Journal of Geodesy*, 81, 679-683. <https://doi.org/10.1007/s00190-007-0135-3>
- Geo++ 2020, State Space Representation Format (SSRZ) Version 1.0
- Japan Cabinet Office 2020, Quasi-Zenith System Interface Specification Centimeter Level Augmentation Service (IS-QZSS-L6-003)
- Kim, M.-S. 2016, Development of PPP Algorithms based on GPS Code Pseudoranges by Applying Real-Time SSR Corrections, Master's Degree, Inha University, South Korea
- Klobuchar, J. 1987, Ionospheric Time-Delay Algorithm for Single-Frequency GPS Users, *IEEE Transactions on Aerospace and Electronic System*, AES-23, 325-331. <https://doi.org/10.1109/TAES.1987.310829>
- Niell, A. E. 1996, Global mapping functions for the atmospheric delay at radio wavelengths, *Journal of Geophysical Research*, 101(B2), 3327-3246. <https://doi.org/10.1029/96JD02107>

org/10.1029/95JB03048

SAPCORDA 2020a, Safe Position Augmentation for Real-Time Navigation (SPARTN) Interface Control Document Version 1.8.0

SAPCORDA 2020b, Safe and Precise Augmentation Service Datasheet Version 1.4

SAPCORDA SAPA Service [Internet], cited 2021 Jan 27, available from: <https://www.sapcorda.com/sapa-services/>

SPARTN Format [Internet], cited 2021 Jan 27, available from: <https://www.spartnformat.org/>

Vana, S., Aggrey, J., Bisnath, S., Leandro, R., Urquhart, L., et al. 2019, Analysis of GNSS correction data standards for the automotive market, *Navigation*, 66, 577-592. <https://doi.org/10.1002/navi.323>



Kwan-Dong Park received his Ph. D. degree from the Department of Aerospace Engineering and Engineering Mechanics at the University of Texas at Austin, and he is currently at Inha University as a professor. His research interests include PPP-RTK algorithm development and GNSS geodesy.



Yeong-Guk Kim received M.S. degree in Geoinformatic Engineering from Inha University, Korea. He received B.S degree from the same university. His research interests include SBAS/PPP-RTK and self-driving cars.



Hye-In Kim received her Ph. D. degree from the Geoinformatic Engineering at the Inha University, and she is currently at PP-Solution Inc. as a director. Her research interests include DGNS/PPP-RTK, positioning and navigation systems, receiver.



Hae-Chang Lee received M.S. degree in Future Vehicle Engineering from Inha University, Korea. He received B.S. degree from the same university. His research interests include CLAS/PPP-RTK and self-driving cars.



Miso Kim received M. S. degree in Geoinformatic Engineering from Inha University, and she is currently working at Research Institute of PP-Solution Inc. Her research interests include GNSS PPP-RTK algorithm development and modeling of GNSS error sources.